Electronic Supplementary Information

Direct Observation of Layered-to-Spinel Phase Transformation in Li_2MnO_3 and Spinel Structure Stabilised after the Activation Process

Keiji Shimoda,*[a] Masatsugu Oishi,‡[a] Toshiyuki Matsunaga,[a] Miwa Murakami,[a] Keisuke Yamanaka,[b] Hajime Arai,[a] Yoshio Ukyo,[a] Yoshiharu Uchimoto,[c] Toshiaki Ohta,[b] Eiichiro Matsubara,[d] Zempachi Ogumi[a]

[a]*Office of Society-Academia Collaboration for Innovation, Kyoto University, Uji, Kyoto 611-0011, Japan*

[b]*SR Censter, Ritsumeikan University, Kusatsu, Shiga 525-8577, Japan*

[c]*Graduate School of Human and Environment Studies, Kyoto University, Kyoto 606-8501, Japan*

[d]*Department of Materials Science and Engineering, Kyoto University, Kyoto 606-8501, Japan*

‡ Present address: Institute of Science and Technology, Tokushima University, Tokushima 770-8506, Japan

*Corresponding author: Keiji Shimoda

Gokashou, Uji 611-0011, Japan

Office of Society-Academia Collaboration for Innovation, Kyoto University

E-mail address: k-shimoda@saci.kyoto-u.ac.jp

Tel: +81-774-38-4967 Fax: +81-774-38-4996

Table S1. Sample list of the Li_2MnO_3 electrode disassembled for structural analyses.

	Sampling point	Potential / V	Capacity /mA h g^{-1} [a]	Li content x in Li_xMnO_3 [b]
1st cycle	#1	–	0.0	2.00
	#2	4.48	115.1	1.50
	#3	4.53	229.4	1.00
	#4	4.60	345.0	0.49
	#5	4.80	448.1	0.04
	#6	3.11	–110.1	0.49
	#7	2.00	–200.9	0.94
2nd cycle	#8	3.63	100.0	0.54
	#9	4.50	229.0	–0.03
	#10	4.80	497.9	–1.17
	#11	2.00	–185.3	0.26
20th cycle	#12	2.00	–139.2	–0.81
21st cycle	#13	4.80	131.3	–1.22

[a] Table S1 lists the individual electrode samples disassembled from different cells, and their capacity values may slightly deviate from Fig. 1 and 6 in the main text. Discharging capacities are expressed as negative values.

[b] Li contents in Li_xMnO_3 are estimated from the observed capacities with respect to the theoretical capacity of 459 mA h g^{-1}. The Li contents estimated for the samples on and after the 2nd charging to 4.8 V (#10–13) are significantly reduced to negative values, which are fictitious due to an additional charging capacity in the 2nd cycle coming from the electrolyte decomposition (Fig. 6).

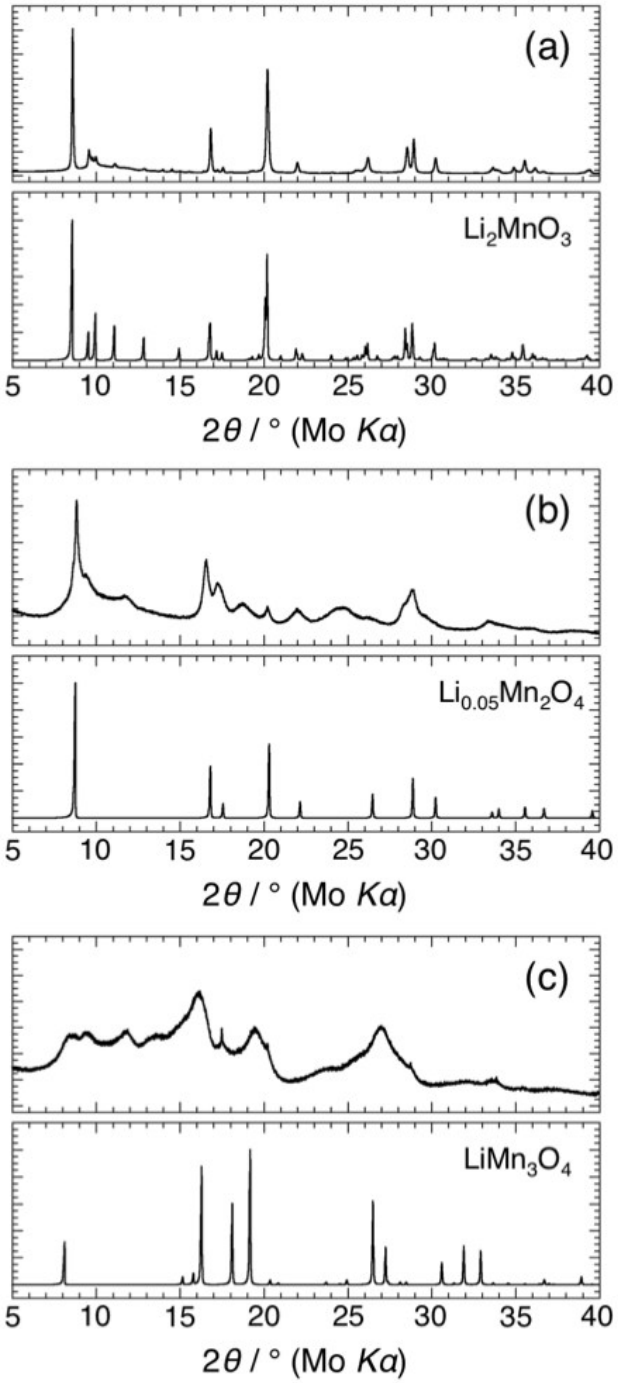

Fig. S1. SR-XRD profiles of (a) pristine electrode (#1), (b) electrode charged to 4.8 V in the 1st cycle (#5), and (c) electrode discharged to 2.0 V in the 20th cycle (#12), along with the simulated profiles for Li_2MnO_3, $Li_{0.05}Mn_2O_4$, and $LiMn_3O_4$, respectively.

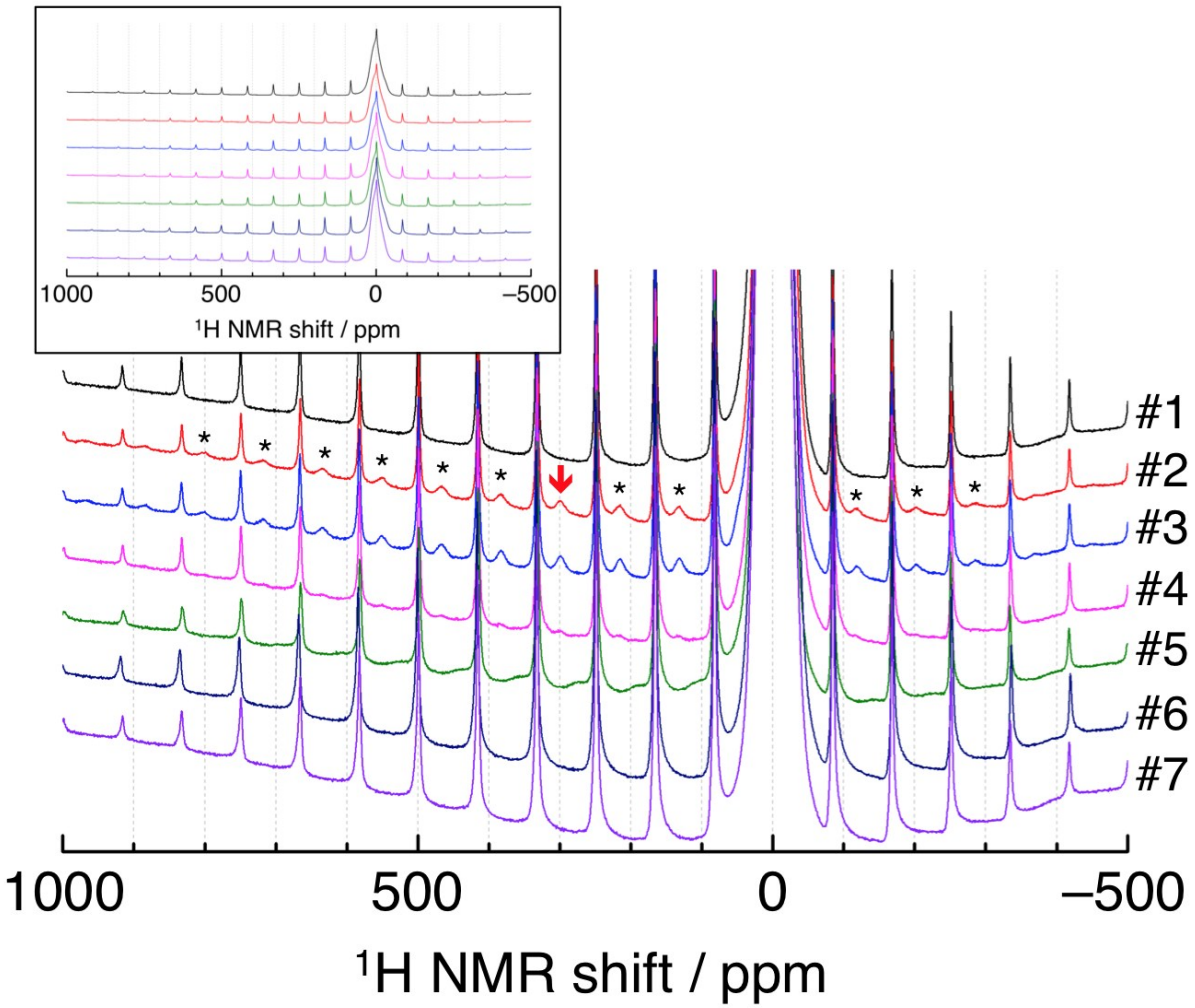

Fig. S2. ^{1}H MAS NMR spectra of the Li_2MnO_3 electrode for the 1st cycle. The signal intensities are normalised to the scan numbers and sample weights in the rotors. For the intercalated proton species, the isotropic signal and its spinning sidebands are marked with arrows and asterisks, respectively. The inset shows overall spectra, which indicate the ^{1}H signal (and its spinning sidebands) coming from PVDF and background components. The sample numbers are listed in Table S1.

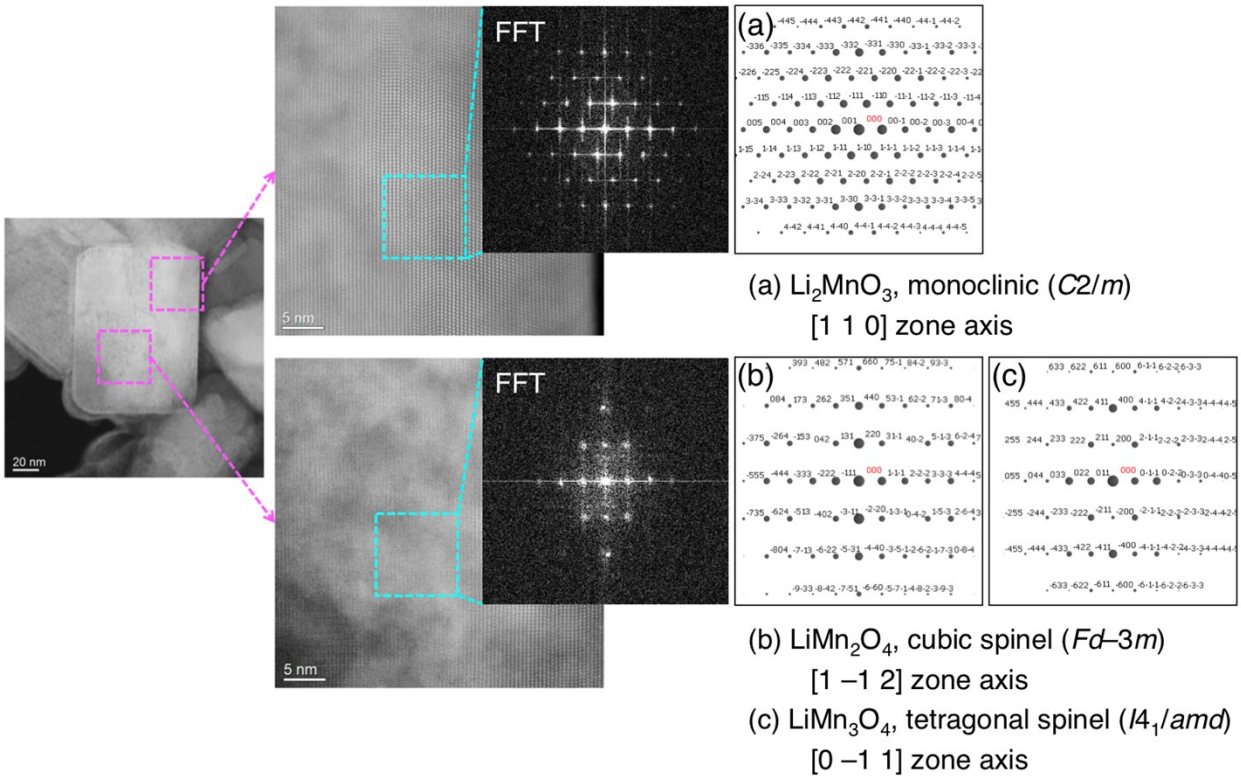

Fig. S3. Atomic column images and their FFT patterns along with the simulated patterns for the electrode sample disassembled at the 50% SOC in the 1st cycle (#3).

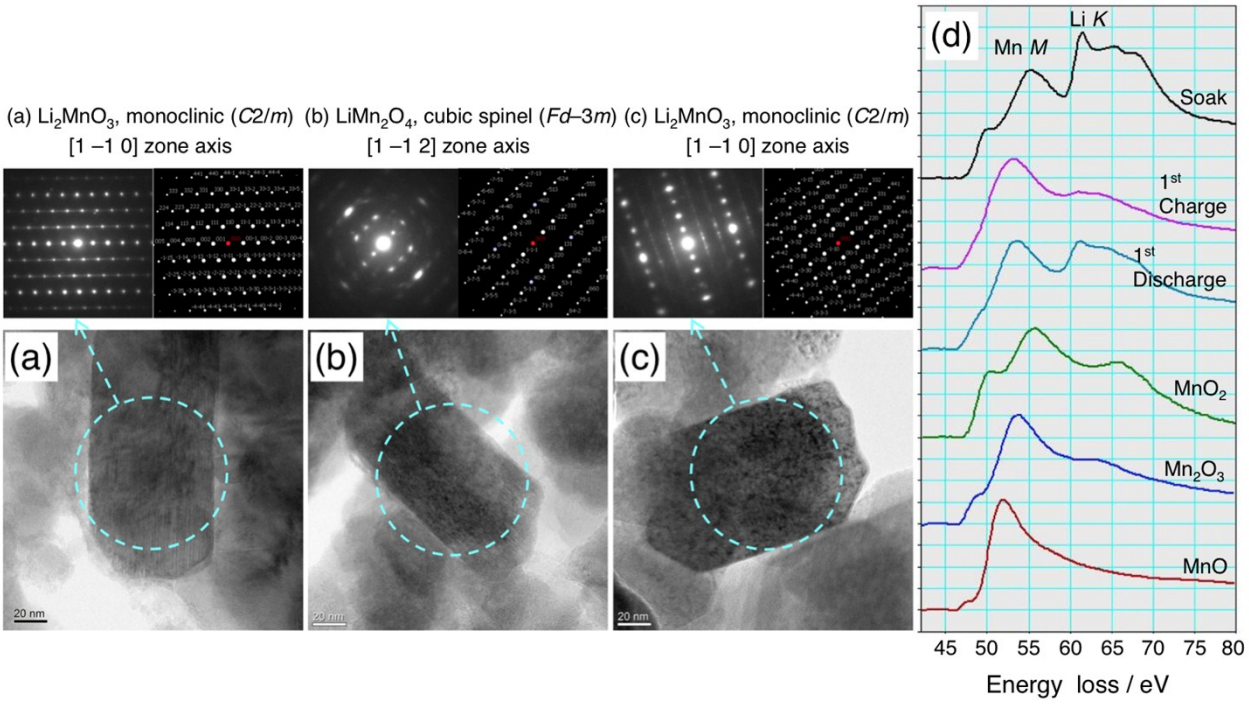

Fig. S4. TEM images and EEL spectra for the electrode samples disassembled after the electrochemical measurements at room temperature. (a) The pristine (soaked) electrode, (b) the electrode charged to 4.8 V in the 1st cycle, and (c) the electrode discharged to 2.0 V in the 1st cycle along with the SAED and simulation patterns. (d) EEL spectra at Mn M-edge + Li K-edge along with the reference materials.

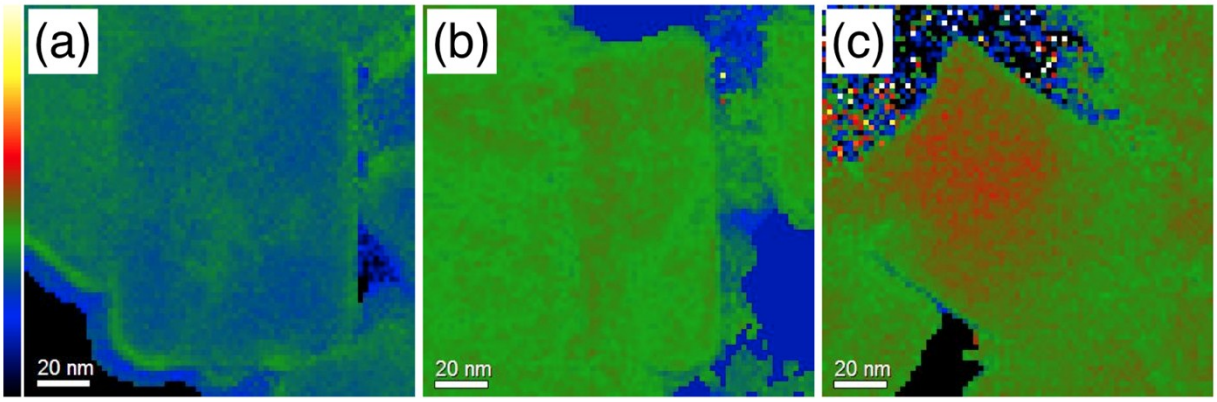

Fig. S5. Mn/(O+Mn) atomic ratio mapping from the O K-edge and Mn L-edge EELS data for the sample disassembled at (a) the 50% SOC in the 1st cycle (#3), (b) 2.0 V in the 20th cycle (#12), and (c) 4.8 V in the 21st cycle (#13), respectively.

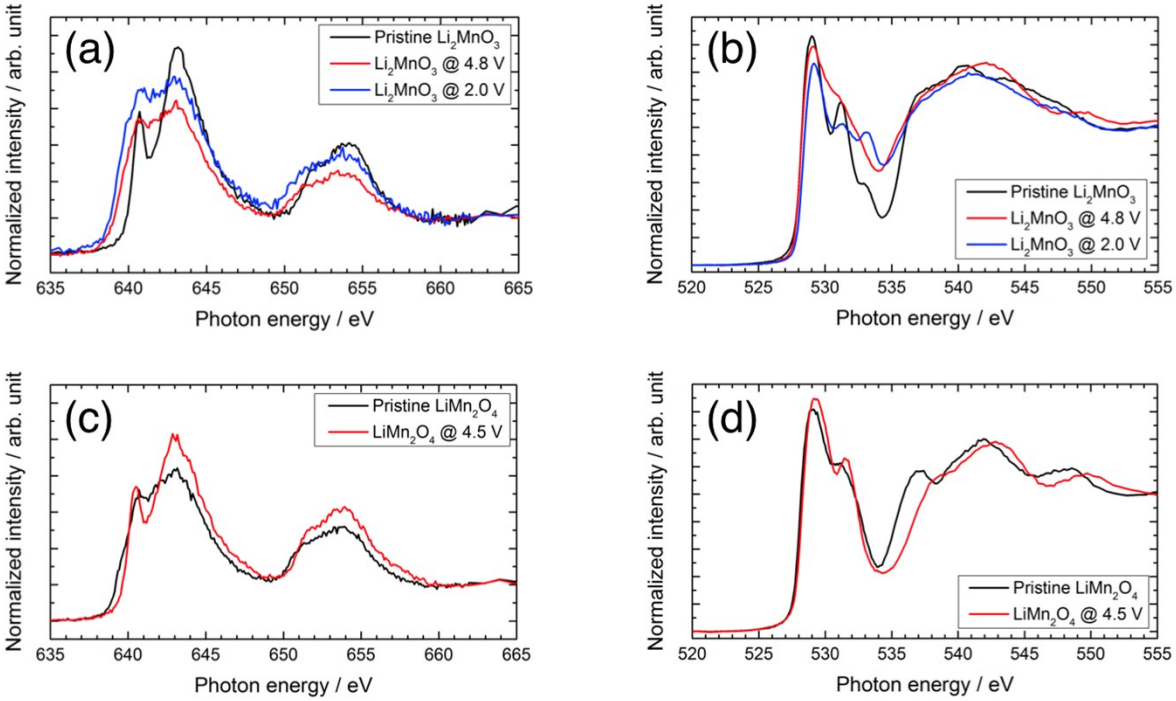

Fig. S6. (a) Mn L- and (b) O K-edge XAFS spectra of the pristine (#1), charged and discharged Li_2MnO_3 samples in the 1st cycle (#5,7) along with (c) Mn L- and (d) O K-edge spectra of the pristine and charged $LiMn_2O_4$ ($Li_{\delta\sim0}Mn_2O_4$) as references. The Mn L- and O K-edge spectra were acquired in the inverse partial fluorescence yield (IPFY) and partial fluorescence yield (PFY) modes, respectively, which are relatively bulk-sensitive with a probing depth of up to ~500 nm, at the beamline BL-11 at the SR Center, Ritsumeikan University (Shiga, Japan). The detailed experimental conditions were described elsewhere.[S1]

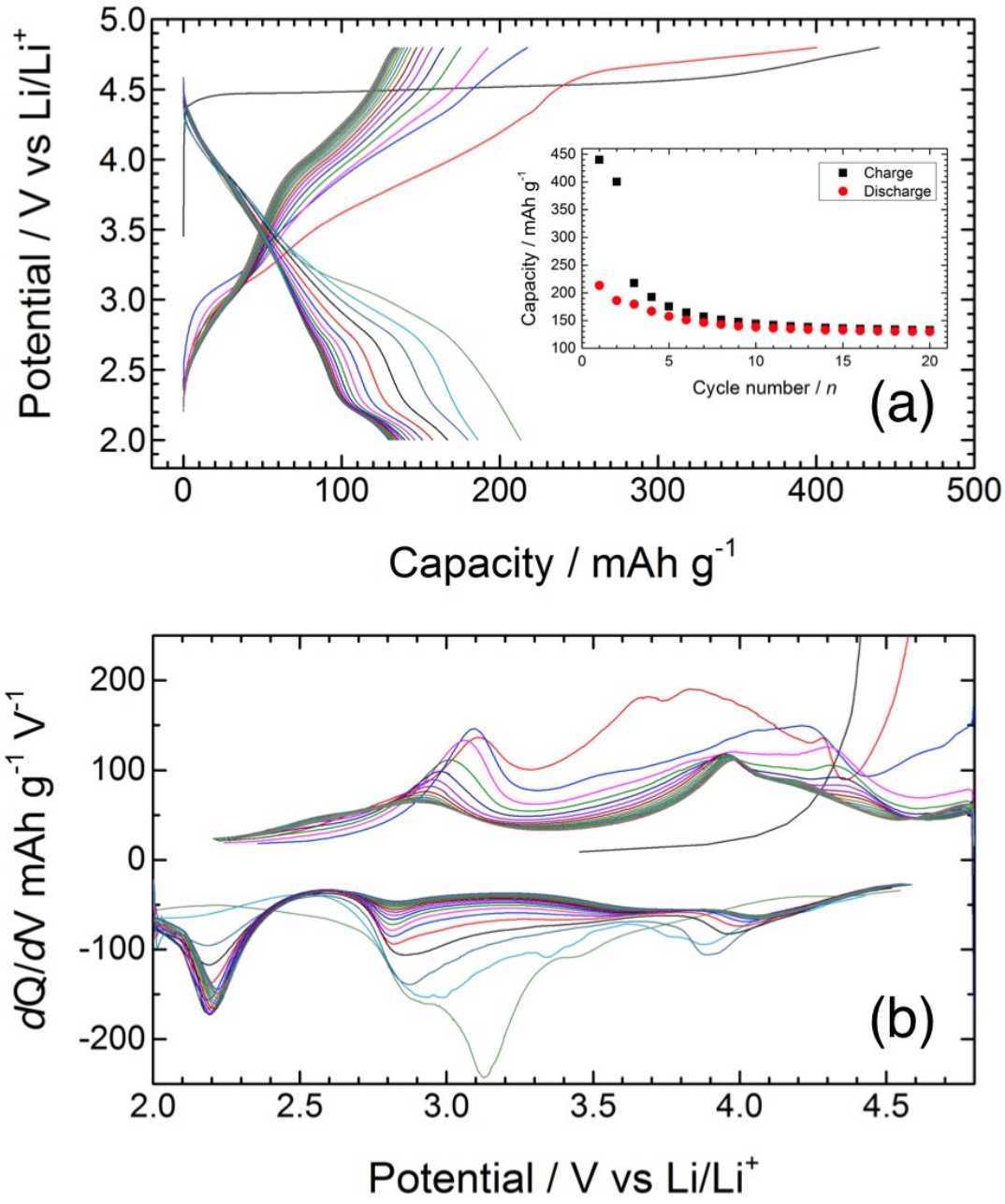

Fig. S7. (a) Charge–discharge profiles of the Li/Li_2MnO_3 cell up to the 20th cycle. The charging and discharging capacities are plotted as a function of cycle number in the inset. (b) dQ/dV curves of the Li/Li_2MnO_3 cell up to the 20th cycle.

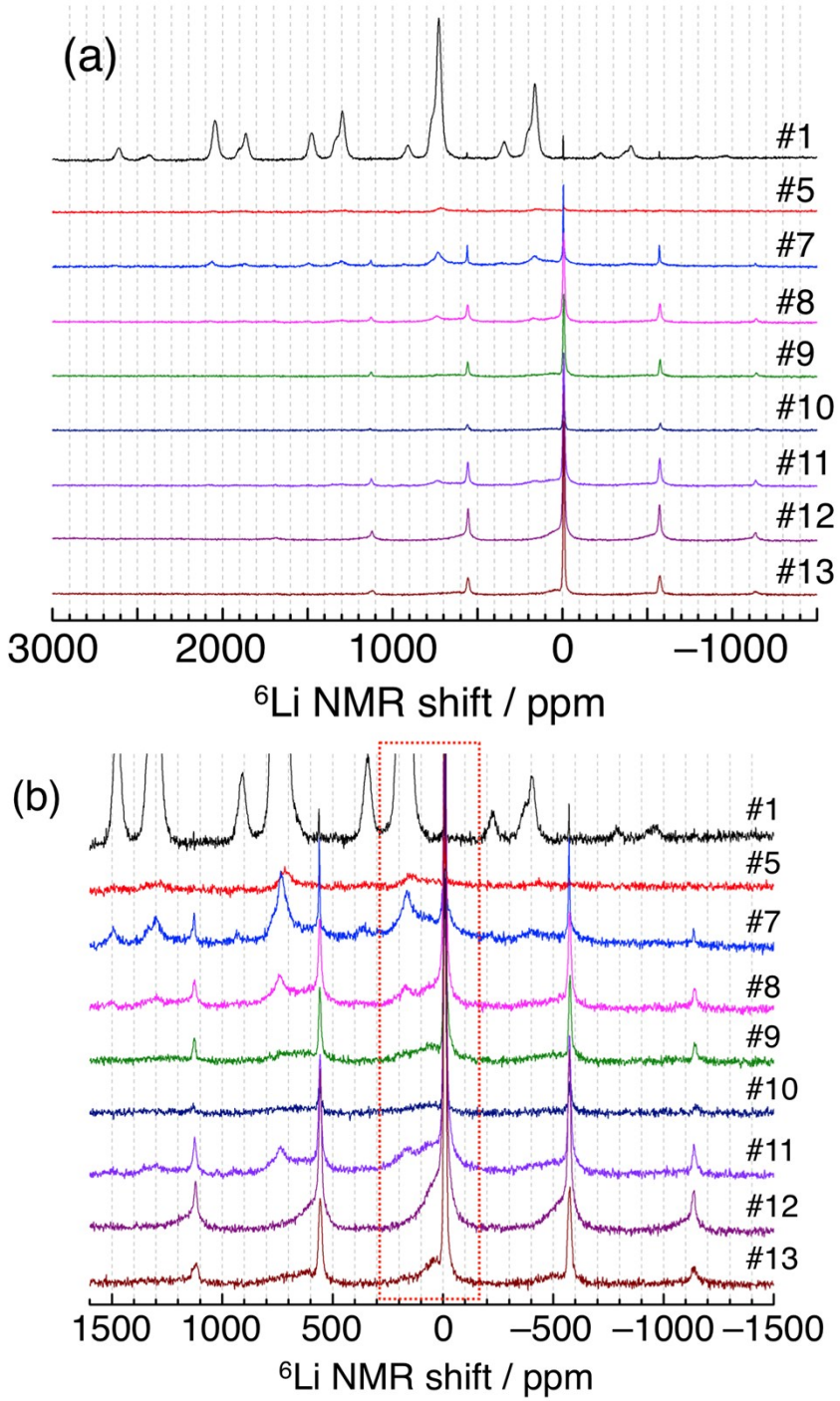

Fig. S8. (a) ^{6}Li MAS NMR spectra of the Li_2MnO_3 electrode for the 1st, 2nd cycles, 20th discharge, and 21st charge. The spectral range between –1500 and 1600 ppm is magnified in (b). After the 1st cycle (#8–13), the broad signal centred at ca. 50 ppm is clearly observed, which is in the resonance

range of those reported for the lithium manganese(III) oxides.[S2,3,4] The sample numbers are listed in Table S1.

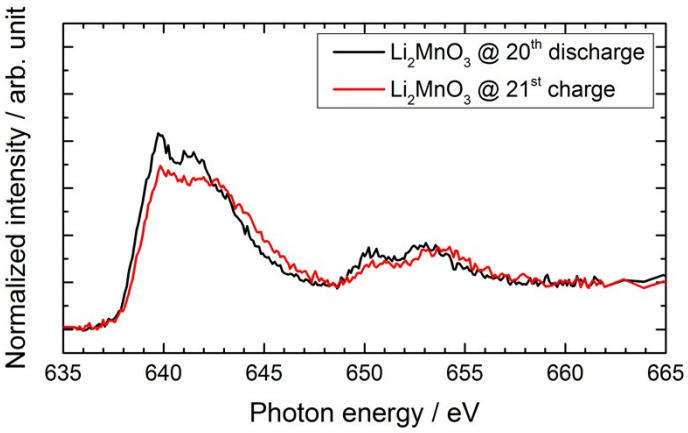

Fig. S9. Mn L-edge XAFS spectra of the Li_2MnO_3 electrode samples discharged in the 20th cycle and charged in the 21st cycle (#12,13).

Supplementary Discussion on the XAFS spectra

Fig. S6 shows the Mn L- and O K-edge XAFS spectra of the pristine, charged and discharged Li_2MnO_3 samples in the 1st cycle. The resulting spectra were almost identical to those in the previous study.[S1] The Mn L-edge spectrum of the pristine sample is similar to that of MnO_2 having the tetravalent Mn ions.[S1] On the other hand, the Li_2MnO_3 electrode samples charged to 4.8 V and discharged to 2.0 V show the spectral shape similar to $LiMn_2O_4$ (Fig. S6c), suggesting some decrease of the Mn oxidation state (+3.5).[S1] This surprising Mn valence reduction on delithiation seems to be associated with the increased pre-edge intensity at 527–534 eV at the O K-edge (Fig. S6b), the latter suggests the increased contribution of the lattice oxygen to charge compensation, that is, the oxidation of lattice oxygen.[S1] This may indicate that the oxygen loss from the structure leads to the charge redistribution in the oxygen-deficient structure, which results in the charge transfer from the lattice oxygen to the Mn ions. During the discharging to 2.0 V, the charge compensation for relithiation is achieved by the reduction of lattice oxygen, whereas the Mn valence state remains as +3.5. These behaviours are different from $LiMn_2O_4$ spinel, where the delithiation/relithiation is compensated by the redox reaction of the Mn ions (Fig. S6c,d).

The Mn L-edge XAFS spectra of the 20th discharged and 21st charged electrode samples are similar to each other (Fig. S9). The centre-of-gravity positions of the L_3 peak at 637–649 eV shift to lower energy compared to those of the 1st charged and discharged electrodes (Fig. S6), indicating that the divalent and trivalent Mn ions become predominant after the multiple charge–discharge cycles. These results lead us to a conclusion that in the degraded material the Mn valence state is reduced and the redox reaction of the Mn ions is less significant to compensate the delithiation/relithiation.

(S1) M. Oishi, K. Yamanaka, I. Watanabe, K.

Shimoda, T. Matsunaga, H. Arai, Y. Ukyo, Y. Uchimoto, Z. Ogumi and T. Ohta, Direct observation of reversible oxygen anion redox reaction in Li-rich manganese oxide, Li_2MnO_3, studied by soft X-ray absorption spectroscopy. *J. Mater. Chem. A*, 2016, **4**, 9293–9302.

(S2) Y.J. Lee and C.P. Grey, ^{6}Li Magic-Angle Spinning (MAS) NMR Study of Electron Correlations, Magnetic Ordering, and Stability of Lithium Manganese(III) Oxides. *Chem. Mater.*, 2000, **12**, 3871–3878.

(S3) C.P. Grey and Y.J. Lee, Lithium MAS NMR studies of cathode materials for lithium-ion batteries. *Solid State Sci.*, 2003, **5**, 883–894.

(S4) J.R. Croy, J.S. Park, F. Dogan, C.S. Johnson, B. Key and M. Balasubramanian, First-Cycle Evolution of Local Structure in Electrochemically Activated Li_2MnO_3. *Chem. Mater.*, 2014, **26**, 7091–7098.